

# Optimised Least Squares Approach for Accurate Polygon and Ellipse Fitting

Yiming Quan<sup>a,b,\*</sup>, Shian Chen<sup>b</sup>

<sup>a</sup>*Department of Civil Engineering, Engineering College, Lishui University, No 1 Xueyuan Road, Lishui, 323000, Zhejiang, China*

<sup>b</sup>*Ningbo Tianyi Design Research of Surveying and Mapping Co. Ltd, 2F Huashang Mansion, No 100 Xinghai South Road, Ningbo, 315040, Zhejiang, China*

---

## Abstract

This study presents a generalised least squares based method for fitting polygons and ellipses to data points. The method is based on a trigonometric fitness function that approximates a unit shape accurately, making it applicable to various geometric shapes with minimal fitting parameters. Furthermore, the proposed method does not require any constraints and can handle incomplete data. The method is validated on synthetic and real-world data sets and compared with the existing methods in the literature for polygon and ellipse fitting. The test results show that the method achieves high accuracy and outperforms the referenced methods in terms of root-mean-square error, especially for noise-free data. The proposed method is a powerful tool for shape fitting in computer vision and geometry processing applications.

*Keywords:* Polygon fitting, Least squares, Rectangle fitting, Ellipse fitting, High-precision

---

## 1. Introduction

Fitting observed points to geometric shapes is a common problem in science and engineering fields. Among various shapes, circle and ellipse fitting has received much attention from researchers [1, 2, 3, 4, 5], and these shape fitting methods have been applied in diverse fields, such as robotics [6], engineering measurement [7, 8], and medicine [9, 10]. Polygon fitting, notably

---

\*corresponding author.

*Email address:* yiming.quan@foxmail.com (Yiming Quan)

rectangles, is equally important for applications in fields such as computer vision [11, 12, 13], medicine [14], and remote sensing [15, 16], where polygonal shapes represent common artifacts. Hence, it is essential to develop generalised and accurate methods for fitting polygons and ellipses to observed data points.

Many studies have attempted to address the problem of fitting polygonal shapes. Some of these methods applied genetic algorithms (GA) to approximate the polygons [14, 17, 18, 19, 20]. Although GA based methods are effective in solving multi-modal optimization problems, the implementation of GA requires more computation resources and is time-consuming. Liparulo et al. [21] proposed to use fuzzy algorithm to reduce the computational cost of point-to-polygon distance estimation, but the main focus of the method was on shape recognition rather than shape fitting. Werman and Keren [22] developed a Bayesian paradigm for parametric and non-parametric fitting of rectangle to noisy data points. Minimum bounding rectangle (MBR), proposed in [23] and [24], has been extensively used for object recognition from LiDAR point clouds [16, 25, 26, 27], images [11, 28, 29, 30, 12], and videos [31, 32]. However, MBR aims to enclose all the points rather than match their distribution.

Least squares methods are widely used for shape fitting. Prasad et al. [3] proposed a fast least squares based ellipse fitting method that does not require constraints and iterations. Chaudhuri et al. [33] introduced a rectangle fit method with a bisection of upper and under-estimated rectangles. The iteration scheme of Chaudhuri's method is based on the computation of rectangle area. However, Yang and Jiang [11] suggested that this method could be improved for discrete and noisy data points, because the area-based fitting metric might not capture the true shape of the data. Another approach to fit rectangle, proposed by Sampath and Shan [34] was to fit line segments and group them by slopes with parallelism, and then determine the bounding by least squares with perpendicularity constraints. Building on Chaudhuri's and Sampath and Shan's work, Seo et al. [15] introduced a rectangle model with eight parameters (angle and distance for each edge) and used least squares adjustment to fit the model to points, subject to the constraint of perpendicularity between edges. Similarly, Sinnreich [35] employed least squares, but reduced the number of parameters to five, corresponding to the degrees of freedom of a symmetrical polygon, and derived a simpler design matrix based on continuous hypotrochoid functions. Stroppa et al. [14] regarded Sinnreich's algorithm as the most effective method for fitting

polygons. However, Stroppa et al. [14] reported that hypotrochoid functions caused errors at the vertices of polygons.

Motivated by these observations, this study introduces a generalised least squares based shape fitting method that seeks to overcome the limitations of the existing methods. The objectives of this paper are to: i) present a generalised fitting algorithm that can be applied to polygons and ellipses; ii) improve the least squares based polygonal fitting algorithm with a more accurate continuous fitness function; iii) test the accuracy of the proposed method in fitting shapes to clean and noisy data. The rest of this paper is organised as follows. Section 2.1 presents the generalised fitness function for polygonal and elliptical shapes. Section 2.3 describes the calculation of the angle parameter in the fitness function. Section 2.4 describes the least squares shape fitting algorithm based on the fitness function. Section 2.5 explains the implementation of the algorithm. Section 3 describes the simulated and real tests, and reports the testing results and analyses. Section 4 concludes the main outcome of this study.

## 2. Least squares polygon and ellipse fitting

### 2.1. A generalised fitness function for unit shapes

Inspired by the Fourier series, we formulated a high-precision trigonometric shape fitting function. We define the 2D regular polygon inscribed by a circle with a diameter of 1 as a unit polygon. Then, the fitness function for a unit polygon with E sides is given by:

$$\begin{aligned} p_x(\phi) &= S\left(\cos \phi\left(a + \frac{b}{\cos(E\phi) + 1.08} - \frac{c}{\cos(2E\phi) + 2}\right) - d \cos((E - 1)\phi)\right) \\ p_y(\phi) &= S\left(\sin \phi\left(a + \frac{b}{\cos(E\phi) + 1.08} - \frac{c}{\cos(2E\phi) + 2}\right) + d \sin((E - 1)\phi)\right) \end{aligned} \quad (1)$$

where the values of parameters a, b, c, d, and S depend on the number of sides E and are listed in Table 1. The function approximates the unit shape precisely with an angle parameter  $\phi$ . Thus, we can implement a simple and computationally efficient least squares algorithm to fit 2D shapes of any position and size, without any constraint conditions. Fig. 1 show the fitness functions for a unit triangle, square, pentagon, and hexagon with calculated root-mean-square error (RMSE).

Table 1: Values of parameters a, b, c, d, and S for unit polygons and ellipse in Eqs. (1)

Unit shape	a	b	c	d	S
Triangle	17	0.14	0.42	5	1/24
Square	15	0.105	0.21	2	1/26
Pentagon	13	0.065	0.13	1	1/24
Hexagon	10	0.0375	0.0675	0.5	1/19
Circle	1	0	0	0	1/2

### 2.2. Shape parameters and error function

Based on the unit shape presented in Eq. 1, we can parameterise corresponding symmetrical and asymmetrical shapes with a vector of six parameters represented by:

$$\mathbf{V} = [x_c \ y_c \ m_x \ m_y \ \alpha \ \lambda]^T \quad (2)$$

where  $x_c$  and  $y_c$  are the coordinates of centroid,  $m_x$  and  $m_y$  are scaling factor to stretch the unit shape along the major and minor axes,  $\alpha$  is a counterclockwise rotation angle, and  $\lambda$  is the shear factor.

Then we can fit polygons or ellipses to the data points by minimizing the error function given by:

$$\begin{aligned} \mathbf{L} &= [\mathbf{L}_1 \ \mathbf{L}_2 \ \cdots \ \mathbf{L}_n]^T, \\ \mathbf{L}_i &= \mathbf{R}^T(\mathbf{X}_i - \mathbf{T}) - \mathbf{M} \cdot \mathbf{P}_i \end{aligned} \quad (3)$$

where  $\mathbf{R}$  is the rotation matrix corresponding to  $\alpha$ ,  $\mathbf{X}_i=[x_i, y_i]^T$  are the coordinates of data points,  $\mathbf{T}=[x_c, y_c]^T$  is the translation vector, and  $\mathbf{P}_i=[p_x, p_y]^T$  is the unit shape defined in Eqs. (1).  $\mathbf{M}$  is defined as follows:

$$\mathbf{M} = \begin{bmatrix} m_x & 0 \\ \lambda m_y & m_y \end{bmatrix} \quad (4)$$

### 2.3. Estimation of the angle parameter $\phi$

To fit the shape using least squares adjustment, a key step is to calculate the intermediate parameter  $\phi$  in Eq. 1 for each data point. A solution of  $\phi$  can be computed for polygon and ellipse through Eqs. 5 to 9 .

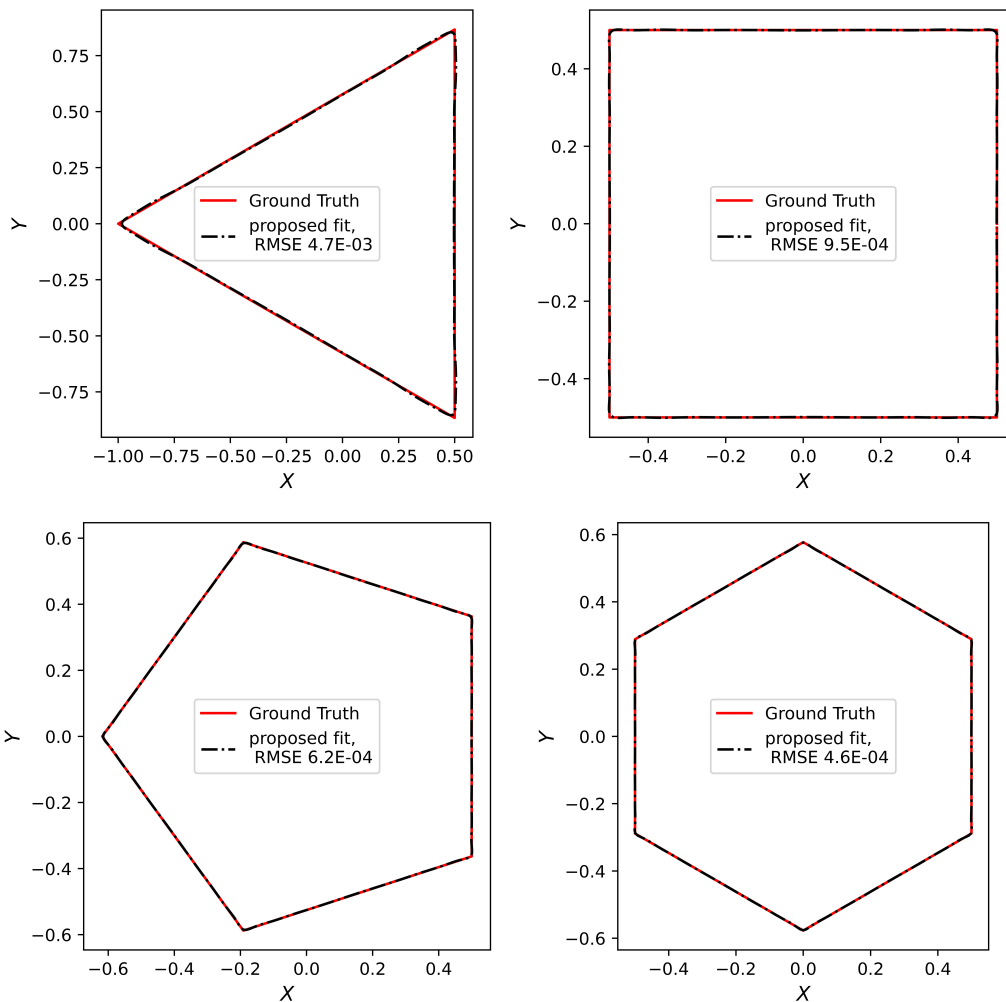


Figure 1: Fitness functions for unit triangle, square, pentagon, hexagon, and ellipse based on Eqs. (1) with RMSE of fitting between the fitness functions and the unit shapes

We denote  $r = p_y/p_x$ , and set  $\theta = \arctan((y_i - y_c)/(x_i - x_c)) - \alpha$ . From Eq. 3 we can have:

$$r = \frac{p_y}{p_x} = -\lambda + \tan \theta \frac{m_x}{m_y} \quad (5)$$

We denote  $w = a/d$ , where  $a$  and  $d$  are the parameters of the fitness function in Eq. 1, and use shorthand notations  $\mathbf{c} = \cos(\phi)$  and  $\mathbf{c}_n = \cos(n\phi)$ .

From Eq. 1 we can get an approximation of  $\cos(\phi)$  for polygon as follows:

$$(r^2 + 1)(w^2 \mathbf{c}^2 + \mathbf{c}_{E-1}^2 - 2w\mathbf{c}\mathbf{c}_{E-1}) + 2w\mathbf{c}_E - w^2 - 1 = 0 \quad (6)$$

where  $E$  is the number of sides of the corresponding unit polygon. From Eq. 6, we can always find two real solutions,  $c_0$  and  $c_1$ , for  $\cos \phi$ . We assume  $c_0 < c_1$  and the correct solution  $c_t$  can be selected based on  $\theta$  by:

$$c_t = \begin{cases} c_0, & \text{for } \cos \theta < 0 \\ c_1, & \text{otherwise} \end{cases} \quad (7)$$

Taking shear factor  $\lambda$  in Eq. 3 into consideration,  $\phi$  can be calculated by taking the inverse cosine of  $c_t$  and adjusting the sign with Eq. 8 for polygon.

$$\phi = \text{sgn}(\sin(\theta - \arctan(\frac{\lambda m_y}{m_x}))) \arccos(c_t) \quad (8)$$

where  $\text{sgn}(\cdot)$  is the sign function.

For ellipse,  $\phi$  can be calculated with Eq. 9.

$$\phi = \arctan(\frac{m_x}{m_y} \tan \theta) + \text{sgn}(\sin \theta) \text{stp}(\cos \theta) \pi \quad (9)$$

where  $\text{stp}(\cdot)$  is a step function defined as:

$$\text{stp}(x) = \begin{cases} 0; & \text{if } x \geq 0 \\ 1; & \text{if } x < 0 \end{cases} \quad (10)$$

In practical implementation, we can simplify the computation of the angle parameter  $\phi$  based on the above equations. Taking rectangle fitting as an example, setting  $w = a/d = 7.5$  from Table 1, Eq. 6 gives:

$$16(r^2 + 1)\mathbf{c}^6 - (84r^2 - 36)\mathbf{c}^4 + (110.25r^2 - 9.75)\mathbf{c}^2 - 42.25 = 0 \quad (11a)$$

Taking  $\lambda = 0$  into Eq. 5 and setting  $k = 1/(r^2 + 1)$ , Eq. 11a can be reduced to:

$$\mathbf{c}^6 + (7.5k - 5.25)\mathbf{c}^4 + (6.890625 - 7.5k)\mathbf{c}^2 - 2.640625k = 0 \quad (11b)$$

From Eq. 11b we can get:

$$c_1 = -c_0 = \sqrt{1.75 - 2.5k - (q_1 + q_2)^{1/3} - (q_1 - q_2)^{1/3}} \quad (11c)$$

where

$$\begin{aligned} q_1 &= p_1(k - 0.5)^3 - p_2(k - 0.5), \\ q_2 &= p_3\sqrt{(k^2 - k)(k - k^2 - p_4)} \end{aligned} \quad (11d)$$

where  $p_1=15.625$ ,  $p_2=5.24609375$ ,  $p_3=8.3998$ ,  $p_4=0.2786875$ . As  $c_1 = -c_0$ , from Eq. 8, the value of  $\phi$  for rectangle can be calculated as follows:

$$\phi = \text{sgn}(\tan \theta) \arccos(c_1) + \text{sgn}(\sin \theta) \text{stp}(\cos \theta) \pi \quad (11e)$$

#### 2.4. Least squares adjustment

With determined shape parameters and error functions described in Section 2.2 and computed  $\phi$  described in Section 2.3, the standard Gauss-Newton method is used to minimise  $\mathbf{L}$ :

$$\mathbf{g} = -(\mathbf{A}^T \mathbf{A})^{-1} \mathbf{A}^T \mathbf{L} \quad (12a)$$

$$\mathbf{V} := \mathbf{V} + \mathbf{g} \quad (12b)$$

where  $\mathbf{A}$  is partial derivatives of  $\mathbf{L}$  given by:

$$\begin{aligned} \mathbf{A} &= [\mathbf{A}_1 \quad \mathbf{A}_2 \quad \cdots \quad \mathbf{A}_n]^T, \\ \mathbf{A}_i &= \begin{bmatrix} \frac{\partial \mathbf{L}_i}{\partial x_c} & \frac{\partial \mathbf{L}_i}{\partial y_c} & \frac{\partial \mathbf{L}_i}{\partial m_x} & \frac{\partial \mathbf{L}_i}{\partial m_y} & \frac{\partial \mathbf{L}_i}{\partial \alpha} & \frac{\partial \mathbf{L}_i}{\partial \lambda} \end{bmatrix} \end{aligned} \quad (13)$$

From Eq. (3), we can have:

$$\begin{aligned} \frac{\partial \mathbf{L}_i}{\partial x_c} &= \begin{bmatrix} -\cos \alpha \\ \sin \alpha \end{bmatrix} - \begin{bmatrix} m_x \frac{\partial p_x}{\partial x_c} \\ m_y (\lambda \frac{\partial p_x}{\partial x_c} + \frac{\partial p_y}{\partial x_c}) \end{bmatrix}, \\ \frac{\partial \mathbf{L}_i}{\partial y_c} &= \begin{bmatrix} -\sin \alpha \\ -\cos \alpha \end{bmatrix} - \begin{bmatrix} m_x \frac{\partial p_x}{\partial y_c} \\ m_y (\lambda \frac{\partial p_x}{\partial y_c} + \frac{\partial p_y}{\partial y_c}) \end{bmatrix} \end{aligned} \quad (13a)$$

$$\begin{aligned} \frac{\partial \mathbf{L}_i}{\partial m_x} &= - \begin{bmatrix} p_x + m_x \frac{\partial p_x}{\partial m_x} \\ m_y (\lambda \frac{\partial p_x}{\partial m_x} + \frac{\partial p_y}{\partial m_x}) \end{bmatrix}, \\ \frac{\partial \mathbf{L}_i}{\partial m_y} &= - \begin{bmatrix} m_x \frac{\partial p_x}{\partial m_y} \\ \lambda p_x + p_y + m_y (\lambda \frac{\partial p_x}{\partial m_y} + \frac{\partial p_y}{\partial m_y}) \end{bmatrix} \end{aligned} \quad (13b)$$

$$\frac{\partial \mathbf{L}_i}{\partial \alpha} = \begin{bmatrix} -\sin \alpha (x_i - x_c) + \cos \alpha (y_i - y_c) \\ -\cos \alpha (x_i - x_c) - \sin \alpha (y_i - y_c) \end{bmatrix} - \begin{bmatrix} m_x \frac{\partial p_x}{\partial \alpha} \\ m_y \frac{\partial p_y}{\partial \alpha} \end{bmatrix} \quad (13c)$$

$$\frac{\partial \mathbf{L}_i}{\partial \lambda} = - \begin{bmatrix} m_x \frac{\partial p_x}{\partial \lambda} \\ m_y (p_x + \lambda \frac{\partial p_x}{\partial \lambda} + \frac{\partial p_y}{\partial \lambda}) \end{bmatrix} \quad (13d)$$

### 2.5. Algorithm Implementation

Before applying the proposed method, the data should be preprocessed with the following steps, which are analogous to the data preprocessing in circle fitting [2]:

a) Translate the data points to the origin by subtracting their mean values:  $x'_i = x_i - \bar{x}$  and  $y'_i = y_i - \bar{y}$ , where  $\bar{x}$  and  $\bar{y}$  are sample means of  $x_i$  and  $y_i$ , respectively.

b) Normalize the data by dividing  $x'_i$  and  $y'_i$  by the root mean squared distance,  $d_{\text{rms}}$ , of the translated data points from the origin.

c) For shapes that are elongated or flattened, we recommend to apply singular value decomposition (SVD) to the translated and normalized data points  $\mathbf{u}\mathbf{v}^T = \mathbf{X}'$ , and obtain the angle of the principal axis as the initial estimate of  $\alpha$ .

These steps can reduce rounding error and mis-convergence in iteration. We can start the search of the parameters  $(x_c, y_c, m_x, m_y, \lambda)$  at  $(0, 0, 1, 1, 0)$  with the calculated initial value of  $\alpha$ . To simplify the fitting problem and reduce the computational cost, we may adjust the vector based on the degrees of freedom of the fitted shape. For example, if the fitted shape is a rectangle or an ellipse, the number of parameters in Eq. (2) is reduced to five as  $\lambda$  is fixed to 0. If the fitted shape is a right triangle, then we can fix  $\lambda = \sqrt{3}/3$ . The optimal parameters after iteration are then transformed back by applying the inverse operations of scaling and translation with Eqs. 14.

$$\begin{aligned} x_c &\leftarrow x_c d_{\text{rms}} + \bar{x}, y_c \leftarrow y_c d_{\text{rms}} + \bar{y}, \\ m_x &\leftarrow m_x d_{\text{rms}}, m_y \leftarrow m_y d_{\text{rms}} \end{aligned} \quad (14)$$

Algorithm 1 shows the procedures of data preprocessing and iterative least squares adjustment.

---

**Algorithm 1** Proposed Shape Fit Algorithm

---

```
1: procedure DATA PREPROCESSING
2:   for each  $(x_i, y_i)$  in  $\mathbf{X}$  do
       $x_i \leftarrow (x_i - \bar{x})/d_{\text{rms}}$ 
       $y_i \leftarrow (y_i - \bar{y})/d_{\text{rms}}$ 
3:   Compute  $\alpha_0$  by  $\mathbf{u}, \mathbf{s}, \mathbf{v}^T := \text{svd}(\mathbf{X})$ 
       $\alpha_0 := \arctan(\mathbf{v}^T)$ 
4: procedure ITERATIVE LEAST SQUARES MINIMIZATION
5:   Initialise  $\mathbf{V} := [0, 0, 1, 1, \alpha_0, 0]^T$ ,  $\epsilon := 10^{-6}$ 
6:   while not converged do
7:     Compute  $\phi$  by Eq. (8) for polygon or Eq. (9) for ellipse
8:     Compute  $\mathbf{L}$  by Eq. (3)
9:     Compute  $\mathbf{A}$  by Eq. (13)
10:    Compute  $\mathbf{g}$  by Eq. (12a)
11:    if  $\|\mathbf{g}\| < \epsilon\|\mathbf{V}\|$  then break
12:    else
13:       $\mathbf{V} \leftarrow \mathbf{V} + \mathbf{g}$ 
14: restore  $(x_c, y_c, m_x, m_y)$  in estimated  $\mathbf{V}$  by Eqs. (14)
```

---

### 3. Validation

#### 3.1. Data Description

We designed four tests to validate our proposed method with different types of data and shapes. Tests 1 and 2 used synthetic data of eleven shapes with varying parameters shown in Table 2. The data points used in Test 1 were corrupted by Gaussian noise with a standard deviation of 0.5 to simulate measurement errors. The data points used in Test 2 were noise-free but partially missing. We deliberately removed some points near vertices of polygons and some points on one side of each ellipse to create gaps in the data. This way, we can evaluate the accuracy and robustness of our proposed method to noisy and incomplete data. We also demonstrate that our method does not rely on the vertices of polygons.

Tests 3 and 4 used real data with rectangular and elliptical shapes because they are ubiquitous in the real world and have many applications in computer vision, image processing, and remote sensing. Test 3 used a point cloud of a building obtained by aerial photogrammetry (Fig. 2), which can be approximated by a rectangle. The data was collected by flying a DJI M300 RTK drone equipped with a Zenmuse P1 photogrammetry camera over the building. The true parameters of the rectangle in Test 3 were computed using the planar coordinates of the four corner points of the building. The true coordinates of the building corners were derived from the as-built drawing, which was created based on a total station survey of the building. Test 4 used an image of a shape matching toy with polygonal and circular shapes to demonstrate the versatility of our proposed method. The image was preprocessed by converting it to gray scale, applying a Gaussian filter for smoothing, and extracting shape contours using Canny edge detector before applying our proposed shape fitting method.

In the tests, we compared our proposed method with two existing methods for rectangle and ellipse fitting proposed by Sinnreich [35] and Prasad [3], respectively, when a ground truth reference is available. We used root-mean-square error (RMSE) as the metric to evaluate fitting accuracy of the proposed and referenced methods.

#### 3.2. Results

Test 1 evaluated the accuracy and robustness of our proposed method for fitting geometric shapes to noisy data. Fig. 3 shows that our proposed method and the referenced methods can fit the noisy data points with low

Table 2: Parameters of eleven shapes in Tests 1 and 2

Shape No.	$x_c$	$y_c$	$m_x$	$m_y$	$\alpha/\text{deg}$	$\lambda$	Type
T0	4	43	15	15	35	/	regular triangle
T1	0	17	28	9	100	/	isocetes triangle
T2	15	-4	15	9	270	$\sqrt{3}/3$	right triangle
R0	32	39	19	19	-10	/	square
R1	33	4	8	41	50	/	rectangle
R2	32	21	8	16	80	$\sqrt{3}/2$	rhombus
R3	49	27	15	7	60	0.8	parallelogram
H0	61	47	20	20	15	/	regular hexagon
H1	68	24	24	16	10	0.6	hexagon
E0	52	8	8	12	20	/	ellipse
E1	68	0	32	8	55	/	ellipse

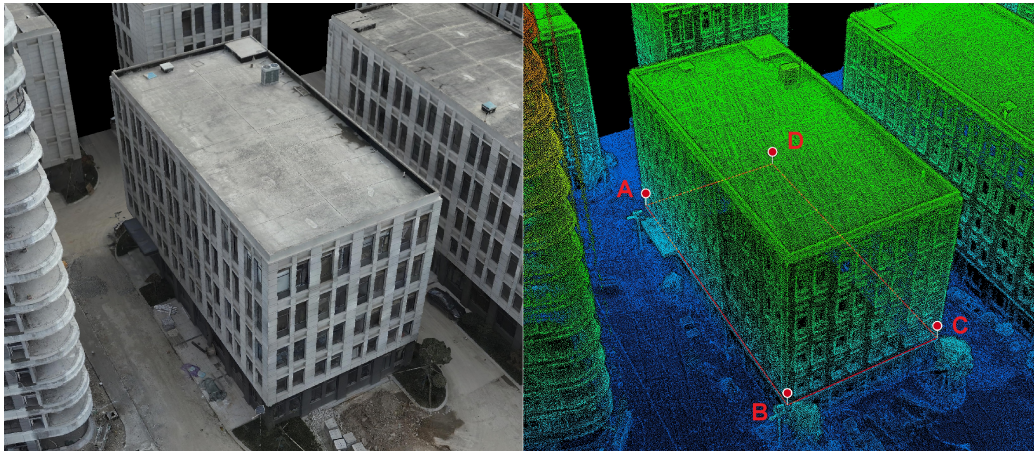


Figure 2: Point cloud of a building from aerial photogrammetry and its 3D model. (a) 3D model of the building. (b) Point cloud of the building. The data used in Test 3 is the sliced point cloud near  $P_{ABCD}$ , which is a plane defined by four corner points of the building.

errors, ranging from 0.5 to 1.3 in RMSE. The estimated parameters and RMSE of fitting points in Test 1 are shown in Table 3. The results show that the RMSE is higher for elongated or flattened shapes such as T1 and R1 because the estimation of a short edge of these shapes is more sensitive to noise. The results also show that our proposed method has similar RMSE as

Sinnreich’s method [35] for rectangle fitting (R0 and R1) and slightly lower RMSE than Prasad’s method [3] for ellipse fitting (E0 and E1). The test results indicate that our method is competitive with the referenced methods, considering that the proposed method is more general and versatile.

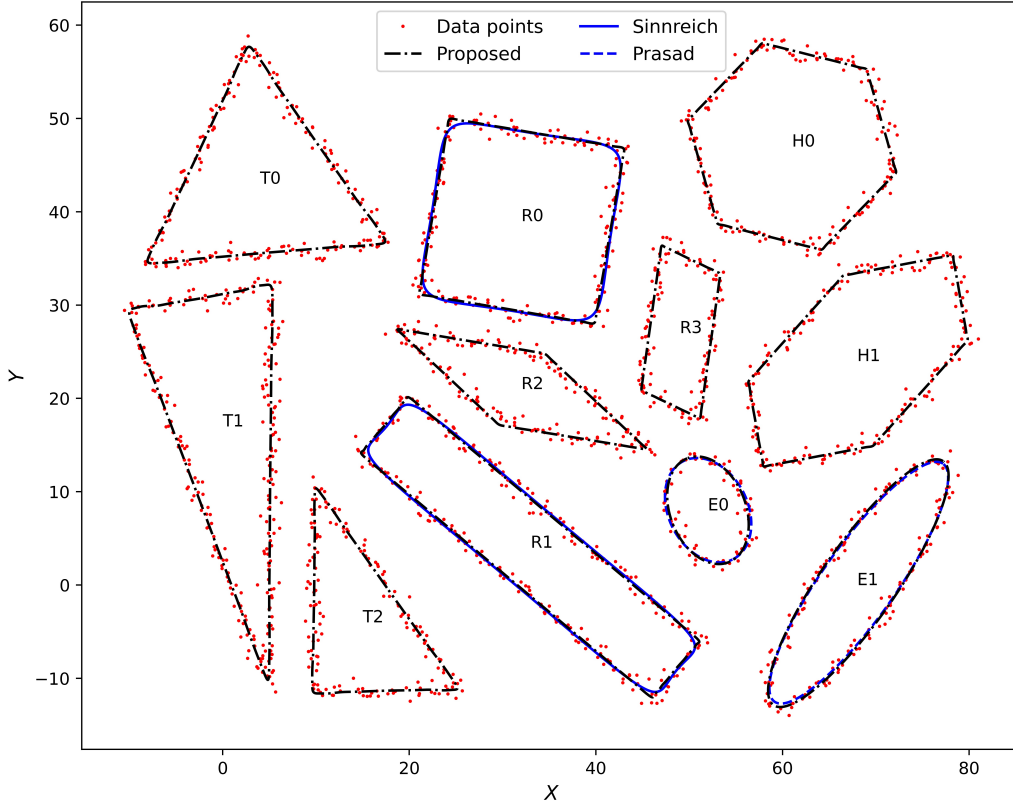


Figure 3: Shape fitting results for noisy points Using proposed and referenced methods in Test 1

Test 2 evaluated the accuracy and robustness of our proposed method for fitting geometric shapes to incomplete data. Fig. 4 illustrates the fitting shapes obtained by the proposed method and referenced methods in Test 2. As shown in Fig. 4, we can see that Sinnreich’s fit of R1 and Prasad’s fit of E1 are slightly smaller than the true shapes, which indicates an underfitting problem. In contrast, our proposed fit matches the data points more closely, which indicates a better fitting accuracy. Table 4 presents the estimated parameters and RMSE of fitting points in Test 2. The RMSE values of our

Table 3: Shape parameter estimation and RMSE for various shapes and methods in Test 1.

Shape	Method	$x_c$	$y_c$	$m_x$	$m_y$	$\alpha/\text{deg}$	$\lambda$	RMSE
T0	Proposed	4.069	43.017	14.964	14.959	154.88	/	0.639
T1	Proposed	0.023	16.989	28.042	9.079	100.08	/	1.122
T2	Proposed	14.963	-4.053	8.701	15.387	35.32	0.199	0.738
R0	Sinnreich	32.038	38.918	19.301	19.158	-8.90	/	0.604
R0	Proposed	32.070	38.995	19.109	19.065	80.39	/	0.550
R1	Sinnreich	33.109	3.931	40.605	8.228	140.08	/	1.295
R1	Proposed	32.958	4.046	40.731	7.998	140.01	/	1.316
R2	Proposed	32.081	20.976	8.940	15.070	46.89	-0.889	1.055
R3	Proposed	49.098	27.118	6.673	15.685	-7.92	-0.136	0.706
H0	Proposed	61.015	47.000	19.945	19.973	16.01	/	0.503
H1	Proposed	68.095	24.026	23.918	16.060	9.98	0.594	0.584
E0	Prasad	52.029	8.014	11.785	8.476	-63.12	/	0.506
E0	Proposed	52.011	8.008	11.985	8.094	111.83	/	0.475
E1	Prasad	68.173	0.245	31.249	7.846	54.71	/	0.781
E1	Proposed	68.128	0.194	31.841	8.043	55.20	/	0.739

proposed method range from 0.009 to 0.074 for polygons, which are lower by 80% and 93% than Sinnreich’s fit. This indicates that the proposed method can handle incomplete data more effectively. For ellipses, the RMSE of the proposed method is exactly zero for these test cases, which indicates that the proposed method can recover the true parameters of the ellipse from incomplete data. Prasad’s fit estimates the centroid and orientation of ellipse correctly, but has a slight error in estimating the major and minor axes of ellipse with incomplete data. This error results in an underfitting problem, as shown in Fig. 4.

It should be noted that some estimated parameters in Table 4 differ from the given parameters in Table 2, even though the corresponding geometric shapes fit well with the data points. For example, Shape R3 has given parameters  $(x_c, y_c, m_x, m_y, \alpha, \lambda) = (49, 27, 15, 7, 60, 0.8)$  in Table 2 and estimated parameters  $(x_c, y_c, m_x, m_y, \alpha, \lambda) = (49.005, 27.018, 6.552, 16.040, -9.6, -0.117)$  in Table 4. This discrepancy is caused by the fact that the parameter model used in Eq. 2 corresponding to an asymmetrical shape has multiple solutions that can produce the same shape.

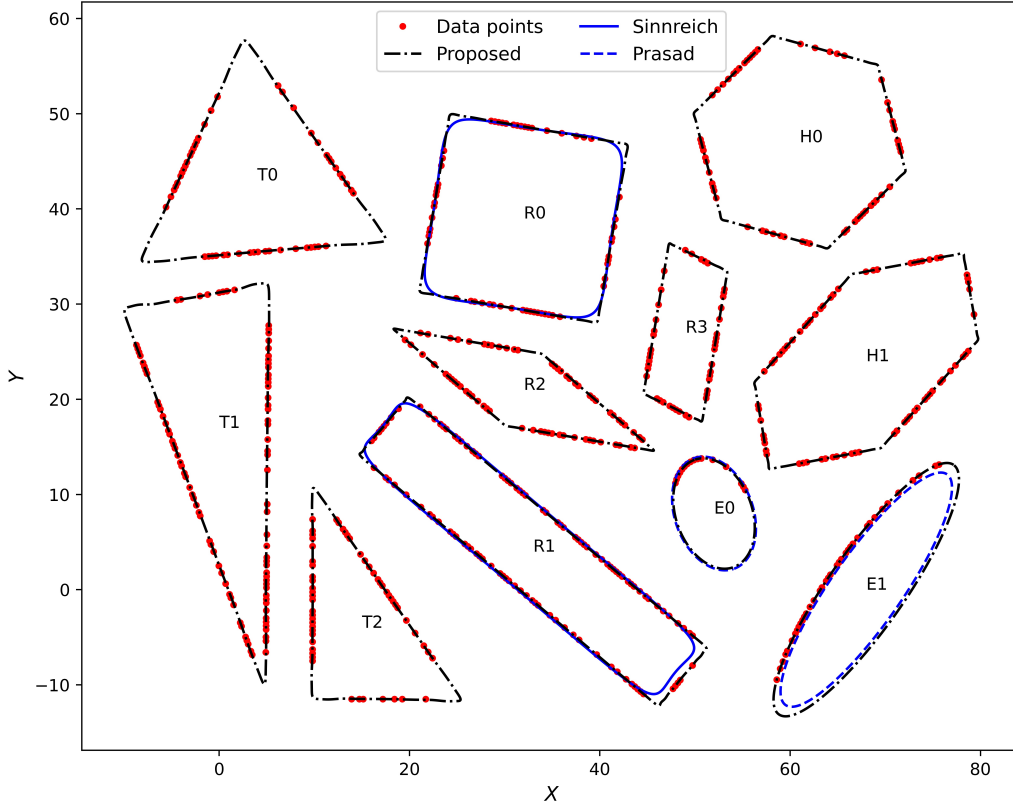


Figure 4: Shape fitting results for noise-free and incomplete points using proposed and referenced methods in Test 2.

The test result using real point cloud data indicates that the proposed method can achieve centimetre level accuracy in high-precision applications. Table 5 shows the estimated parameters and RMSE of fitting points in Test 3. From Table 5, we can observe that the estimated parameters of the proposed fit are close to the ground truth, whilst Sinnreich’s fit overestimates the length of the short edge of the rectangle. Fig. 3 illustrates the fitted shapes by both methods overlaid on the point cloud data. A close look at Fig. 3 shows that Sinnreich’s fit exhibits a slight outward deviation from the long edge of the rectangle except near the vertices, where it curves inward. However, the proposed fit shows closer proximity to the rectangle, especially in capturing the vertices.

Test 4 shows that our proposed method can fit various shapes in a real

Table 4: Shape parameter estimation and RMSE for various shapes and methods in Test 2.

Shape	Method	$x_c$	$y_c$	$m_x$	$m_y$	$\alpha/\text{deg}$	$\lambda$	RMSE
T0	Proposed	4.010	42.982	15.082	14.979	155.09	/	0.039
T1	Proposed	-0.016	17.087	27.912	8.989	100.01	/	0.074
T2	Proposed	15.043	-4.053	8.538	15.883	34.84	0.191	0.043
R0	Sinnreich	31.958	38.996	18.872	18.957	-8.61	/	0.102
R0	Proposed	31.993	39.009	19.017	18.988	80.25	/	0.020
R1	Sinnreich	32.602	4.303	40.171	8.196	139.95	/	0.344
R1	Proposed	32.996	4.002	41.017	8.003	140.00	/	0.023
R2	Proposed	32.002	21.003	8.241	15.656	49.23	-0.870	0.074
R3	Proposed	49.005	27.018	6.552	16.040	-9.60	-0.117	0.066
H0	Proposed	61.001	47.003	20.002	20.000	14.68	/	0.018
H1	Proposed	68.000	24.001	23.935	16.035	9.73	0.603	0.009
E0	Prasad	52.000	8.000	12.346	8.231	-70.00	/	0.157
E0	Proposed	52.000	8.000	12.000	8.000	110.00	/	0.000
E1	Prasad	68.000	-0.000	29.583	7.396	55.00	/	0.643
E1	Proposed	68.000	-0.000	32.000	8.000	55.00	/	0.000

Table 5: Shape parameter estimation and RMSE for the rectangular building in Test 3

Parameters	Ground truth	Sinnreich fit	proposed fit
$x_c/\text{m}$	295595.930	295595.883	295595.947
$y_c/\text{m}$	95593.943	95594.002	95593.912
$m_x/\text{m}$	33.100	32.950	33.112
$m_y/\text{m}$	16.685	17.645	16.743
$\alpha/\text{deg}$	155.77	156.24	155.86
<b>RMSE/m</b>		<b>0.514</b>	<b>0.081</b>

image of a shape-matching toy, which contains incomplete and noisy contours. From Fig. 6b, we can see that some of the contours that belong to different shapes, such as the bottom-left square and top-right rhombus, are not complete. Some edges of shapes are not captured after the image pre-processing because of the changing light reflection along the shape edges in the original image (Fig. 6a). However, the proposed method still works well

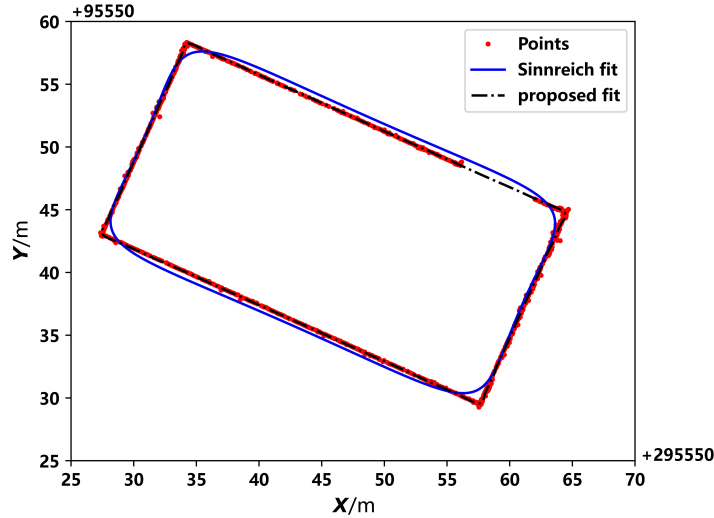


Figure 5: Shape fitting results for real point cloud data using proposed and referenced methods in Test 3.

in fitting all the shapes as shown in Fig. 6c, demonstrating that our method is robust to contour gaps and noise, and versatile to polygonal and circular shapes.

#### 4. Conclusions

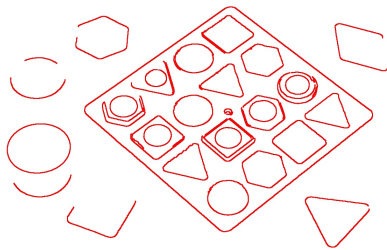
This work has presented a novel method for accurate shape fitting that can handle polygons and ellipses. We validated our method with simulated and real data. The simulated tests show that the proposed method is robust to noisy data and incomplete data. The real data tests further demonstrate the accuracy and versatility of the proposed method to the real-world point cloud data and image data. The proposed method was compared with the existing methods in the literature. The results show that the proposed method achieved higher accuracy and better versatility. The proposed method has potential applications in various fields that involve shape analysis, such as computer vision, image processing, and remote sensing.

#### Acknowledgement

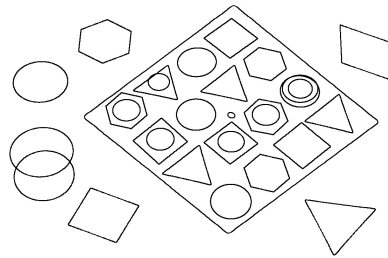
This work was supported by 2021 Science and Technology Projects of Zhejiang Provincial Department of Natural, which is a joint project with



(a) Original image



(b) Input contours as input



(c) Fitting result of proposed method

Figure 6: Example of a real image and the shapes fitted by the proposed method.

Ningbo Tianyi Design Research of Surveying and Mapping Co. Ltd.

## References

- [1] F. Mai, Y.S. Hung, H. Zhong, W. F. Sze, A hierarchical approach for fast and robust ellipse extraction, *Pattern Recognit.* 41 (8) (2008) 2512-2524, doi:10.1016/j.patcog.2008.01.027.
- [2] H. Abdul-Rahman, N. Chernov, Fast and numerically stable circle fit, *J Math Imaging Vis* 116 (2014) 289–295, doi:10.1007/s10851-013-0461-4.
- [3] D.K. Prasad, M.K. Leung, C. Quek, ElliFit: An unconstrained, non iterative, least squares based geometric ellipse fitting method, *Pattern Recognit.* 46 (5) (2013) 1449-1465, doi: 10.1016/j.patcog.2012.11.007.
- [4] T. Wang, Z. Shi, B. Yu, A parameterized geometric fitting method for ellipse, *Pattern Recognit.* 116 (2021) 107934, doi:10.1016/j.patcog.2021.107934.
- [5] R. Maalek, D.D. Lichti, New confocal hyperbola-based ellipse fitting with applications to estimating parameters of mechanical pipes from point clouds, *Pattern Recognit.* 116 (2021) 107948, doi:10.1016/j.patcog.2021.107948.
- [6] H. Dong, E. Asadi, G. Sun, D.K. Prasad, I.-M. Chen, Real-time robotic manipulation of cylindrical objects in dynamic scenarios through elliptic shape primitives, *IEEE Trans. Robot.* (2018) 1–19, doi:10.1109/tro.2018.2868804.
- [7] Y. Quan, L. Lau, Development of a trajectory constrained rotating arm rig for testing GNSS kinematic positioning, *Measurement* 140 (2019) 479-485, doi:10.1016/j.measurement.2019.04.013.
- [8] Z. Lu, B. Liu, K. Zhang, H. Lin and Y. Zhang, A Method for Measuring the Inclination of Forgings Based on an Improved Optimization Algorithm for Fitting Ellipses, *IEEE Trans. Instrum. Meas.* 72 (2023) 1-11, doi: 10.1109/TIM.2022.3221761.
- [9] J. Li, Y. Wang, B. Lei, J.-Z. Cheng, J. Qin, T. Wang, S. Li, D. Ni, Automatic fetal head circumference measurement in ultrasound using random forest and fast ellipse fitting, *IEEE J. Biomed. Health*, 22 (1) (2018) 215-223, doi: 10.1109/JBHI.2017.2703890.

- [10] R. Ranjbarzadeh, S.B. Saadi, Automated liver and tumor segmentation based on concave and convex points using fuzzy c-means and mean shift clustering, *Measurement* 150 (2020) 107086, doi: 10.1016/j.measurement.2019.107086.
- [11] J. Yang, Z. Jiang, Rectangle fitting via quadratic programming, in: 2015 IEEE 17th International Workshop on Multimedia Signal Processing, Xiamen, China, 2015, pp. 1-6, doi: 10.1109/MMSP.2015.7340875.
- [12] Z. Liu, H. Wang, L. Weng, Y. Yang, Ship rotated bounding box space for ship extraction from high-resolution optical satellite images with complex backgrounds, *IEEE Geosci. Remote Sens. Lett.* 13 (8) (2016) 1074–1078, doi: 10.1109/LGRS.2016.2565705.
- [13] J. -C. Bazin, I. Kweon, C. Démonceaux, P. Vasseur, Rectangle extraction in catadioptric images, in: IEEE 11th International Conference on Computer Vision, Rio de Janeiro, Brazil, 2007, pp. 1-7, doi: 10.1109/ICCV.2007.4409208.
- [14] F. Stroppa, C. Loconsole, A. Frisoli, Convex polygon fitting in robot-based neurorehabilitation, *Appl. Soft Comput. J.* 68 (2018) 609-625, doi:10.1016/j.asoc.2018.04.013.
- [15] S. Seo, J. Lee, Y. Kim, Extraction of boundaries of rooftop fenced buildings from airborne laser scanning data using rectangle models, *IEEE Geosci. Remote Sens. Lett.* 11 (2) (2014) 404-408, doi: 10.1109/LGRS.2013.2263575.
- [16] M. Feng, T. Zhang, S. Li, G. Jin, Y. Xia, An improved minimum bounding rectangle algorithm for regularized building boundary extraction from aerial LiDAR point clouds with partial occlusions, *Int. J. Remote Sens.* 41 (2) (2020) 300-319, doi: 10.1080/01431161.2019.1641245.
- [17] P. Yin, A new method for polygonal approximation using genetic algorithms, *Pattern Recognit. Lett.* 19 (1998) 1017-1026, doi:10.1016/s0167-8655(98)00082-8.
- [18] P. Yin, Genetic algorithms for polygonal approximation of digital curves, *Int. J. Pattern Recognit. Artif. Intell.* 13 (7) (1999) 1061-1082, doi:10.1142/S0218001499000598.

- [19] Y. Tsai, Fast polygonal approximation based on genetic algorithms, in: 5th IEEE/ACIS International Conference on Computer and Information Science and 1st IEEE/ACIS International Workshop on Component-Based Software Engineering, Software Architecture and Reuse, 2006, pp. 322–326, doi:10.1109/icis-comsar.2006.39.
- [20] Z. Liu, J. Watson, A. Allen, A polygonal approximation of shape boundaries of marine plankton based-on genetic algorithms, *J. Vis. Commun. Image Represent.* 41 (2016) 305-313, doi:10.1016/j.jvcir.2016.10.010.
- [21] L. Liparulo, A. Proietti, M. Panella, Fuzzy membership functions based on point-to-polygon distance evaluation, in: 2013 IEEE International Conference on Fuzzy Systems, 2013, pp. 1–8, doi:10.1109/fuzz-ieee.2013.6622449.
- [22] M. Werman, D. Keren, A Bayesian method for fitting parametric and non-parametric models to noisy data, *IEEE Trans. Pattern Analysis Mach. Intell.* 23 (5) (2001) 528–534, doi: 10.1109/34.922710.
- [23] H. Freeman and R. Shapira, Determining the minimum-area encasing rectangle for an arbitrary closed curve, *Commun. ACM*, 18 (7) (1975) 409–413, doi:10.1145/360881.360919.
- [24] D. Chaudhuri and A. Samal, A simple method for fitting of bounding rectangle to closed regions, *Pattern Recognit.* 40 (7) (2007) 1981-1989, doi:10.1016/j.patcog.2006.08.003.
- [25] E. Kwak, M. Al-Durgham, A. Habib, Automatic 3D building model generation from lidar and image data using sequential minimum bounding rectangle, *Int. Arch. Photogramm. Remote Sens. Spatial Inf. Sci.*, XXXIX-B3 (2012) 285–290, doi:10.5194/isprsarchives-XXXIX-B3-285-2012.
- [26] E. Kwak, A. Habib, Automatic representation and reconstruction of DBM from LiDAR data using Recursive Minimum Bounding Rectangle, *ISPRS J Photogramm. Remote Sens.* 93 (2014) 171-191, doi:10.1016/j.isprsjprs.2013.10.003.
- [27] M. Kabolizade, H. Ebadi, A. Mohammadzadeh, Design and implementation of an algorithm for automatic 3D reconstruction of building models

- using genetic algorithm, *Int. J. Appl. Earth Obs. Geoinf.* 19 (2012) 104-114, doi:10.1016/j.jag.2012.05.006.
- [28] Y. Wang, L. Wang, H. Lu, Y. He, Segmentation based rotated bounding boxes prediction and image synthesizing for object detection of high resolution aerial images, *Neurocomputing*, 388 (2020) 202-211, doi:10.1016/j.neucom.2020.01.039.
- [29] G.-S. Xia, X. Bai, J. Ding, Z. Zhu, S. Belongie, J. Luo, M. Datcu, M. Pelillo, L. Zhang, Dota: a large-scale dataset for object detection in aerial images, in: *Proceedings of the IEEE Conference on Computer Vision and Pattern Recognition (CVPR)*, 2018.
- [30] J. Ding, N. Xue, Y. Long, G.-S. Xia, Q. Lu, Learning RoI transformer for detecting oriented objects in aerial images, in: *Proceedings of the IEEE Conference on Computer Vision and Pattern Recognition (CVPR)*, 2019.
- [31] A. Edgcomb, F. Vahid, Automated fall detection on privacy-enhanced video, in: *2012 Annual International Conference of the IEEE Engineering in Medicine and Biology Society*, San Diego, CA, USA, 2012, pp. 252-255, doi: 10.1109/EMBC.2012.6345917.
- [32] W.-C. Hu, C.-H. Chen, T.-Y. Chen, D.-Y. Huang, Z.-C. Wu, Moving object detection and tracking from video captured by moving camera, *J. Vis. Commun. Image Represent.* 30 (2015) 164-180, doi:10.1016/j.jvcir.2015.03.003.
- [33] D. Chaudhuri, N. K. Kushwaha, I. Sharif, A. Samal, Finding best-fitted rectangle for regions using a bisection method, *Mach. Vis. Appl.* 23 (6) (2011) 1263–1271, doi:10.1007/s00138-011-0348-6.
- [34] A. Sampath, J. Shan, Building boundary tracing and regularization from airborne lidar point clouds, *Photogramm. Eng. Remote Sens.* 73 (7) (2007) 805–812, doi:10.14358/PERS.73.7.805.
- [35] J. Sinnreich, Least-squares fitting of polygons, *Pattern Recognit. Image Analysis* 26 (2) (2016) 343-349, doi:10.1134/S10546618160202180.